Arsenic Detection

DOI: 10.1002/ange.200800776

Surface-Enhanced Raman Spectroscopy for Trace Arsenic Detection in Contaminated Water**

*Martin Mulvihill, Andrea Tao, Kanokraj Benjauthrit, John Arnold, and Peidong Yang**

Low-level arsenic contamination of drinking water in Bangladesh, India, and parts of China presents an international public health crisis, with over 300000 deaths attributed to chronic poisoning in Bangladesh alone. In 1993, the World Health Organization set a provisional guideline of 10 ppb (0.01 mg L^{-1}) for maximum arsenic content in groundwater.[1] However, exposure to arsenic at these concentrations still results in increased rates of skin, lung, urinary bladder, and kidney cancer.[1] New technologies allowing reliable detection of arsenic below 10 ppb should instigate a stricter standard. Current technologies for laboratory analysis (e.g. inductively coupled plasma (ICP) MS, atomic fluorescence spectroscopy (AFS), HPLC-MS) allow detection at these levels, but they are neither readily available in developing countries nor capable of on-site field detection.[2,3] The current state of field-compatible technologies has been reviewed, and there remains significant room for improvement.[3,4] Even if current chemical field tests are improved to meet these standards, there are no examples of chemical indicators that can distinguish the oxidation state of the arsenic species. For exposure studies, this knowledge is necessary for toxicology, remediation, and monitoring of the effects within the local populations. By developing a highly active substrate for surface-enhanced Raman spectroscopy (SERS) that can be used in conjunction with portable Raman technology,[5] many of these challenges can be surmounted.

Since the discovery of SERS in the late 1970s there has been a continual push to maximize the Raman signal for molecules near nanostructured surfaces. SERS enhancement results from an intense local amplification of the electric field near a metal surface when collective oscillations of conduction electrons resonate in phase with the incident light. The size, shape, and proximity of nanostructures all affect the frequency and magnitude of the localized surface plasmons (LSPs),[6,7] thus directly influencing the degree of Raman enhancement exhibited. LSPs have been directly observed using experimental techniques such as scanning near field[8] and TEM-correlated dark field[9] microscopy. These experiments, along with more conventional light-scattering techniques, demonstrate the dramatic effects that size and shape have on the LSPs.[7] Recent studies on electromagnetic coupling between nanostructures that are nearly touching indicate that such collective effects can excite LSPs that lead to even higher electromagnetic enhancement.[10–13] Although it is widely known that silver shows the strongest plasmonic response,[7] gold is often used for sensing applications because of its chemical stability and compatibility with many laser excitation wavelengths.[14] For our SERS sensor, we have introduced two key features that lead to better analytical capability under typical sensing conditions. First, dense arrays of silver nanocrystals are fabricated using Langmuir–Blodgett (LB) assembly. These close-packed monolayers exhibit broadband scattering profiles, making them compatible with many different excitation wavelengths.[13] The second key feature is the surface passivation of the silver particles with adsorbed polymer. Surface-adsorbed poly(vinyl pyrrolidone) (PVP) serves dual purposes: it functions as the passivating ligand during nanocrystal synthesis, and it stabilizes the silver particles to oxidation while still facilitating interaction between silver and arsenate during sensing experiments. The PVP coating makes these silver nanostructures air- and water-stable over much longer periods then other passivating ligands.

The synthesis of the polyhedral silver nanoparticles proceeds by the polyol process, in which the metal-salt precursors and a polymer capping agent (PVP) are alternately added to a solution of pentanediol heated near reflux.[15] In this way the pentanediol acts as both the solvent and the reductant for the reaction, while PVP imparts shape control as the particles grow.[16,17] The final shape of the particles is dictated by the length of the reaction; the particles are progressively capped by more [111] faces (see Figure 1). This growth results in an increase of the particle size as the reaction progresses, starting with cubes which are 80–100 nm on an edge, then cuboctahedra with diameters of 150–200 nm, and finally octahedra with edge lengths of 250–300 nm. Typically these nanocrystals can be isolated as nearly monodisperse suspensions, and final purification is achieved by filtration through 0.45-μm Durapore filters. Homogeneity of

[*] M. Mulvihill, K. Benjauthrit, Prof. J. Arnold, Prof. P. Yang
Department of Chemistry
University of California, Berkeley
Berkeley, CA 94720 (USA)
Fax: (+1) 510-642-7301
E-mail: p_yang@berkeley.edu
Dr. A. Tao
Institute for Collaborative Biotechnologies
University of California, Santa Barbara
Santa Barbara, CA 93106 (USA)

[**] The authors would like to thank David Okawa and Prof. Alex Zettl for granting use of their multiple wavelength Renishaw MicroRaman instrument. We would like to thank Allan Smith for helpful discussions and Craig Steinmaus for providing the well-water samples and AFS data. Additionally, we would like to acknowledge the NIEHS Superfund Basic Research Program and the U.S. Department of Energy under Contract No. DE-AC02-05CH11231 for funding.

Supporting information for this article is available on the WWW under http://dx.doi.org/10.1002/anie.200800776.

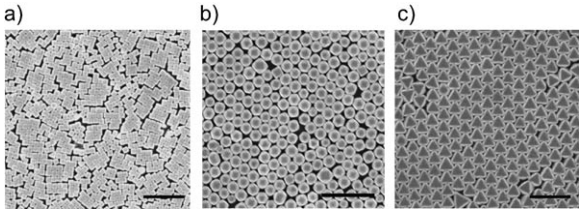

Figure 1. Scanning electron microscopy (SEM) images showing close-packed films of the three nanocrystal shapes: a) cubes, b) cuboctahedra, and c) octahedra; scale bars are 1 μm.

size and shape are essential to obtain well-ordered close-packed monolayers using the LB technique.

For a typical nanoparticle assembly, PVP-coated nanoparticles are dispersed on the water surface of a LB trough with subsequent compression of a mobile barrier.[18] The surface pressure of the film is monitored, and it is transferred to a silicon wafer at a surface pressure of 14 mN cm^{-2} (Figure 1). Once transferred to the silicon wafer, the PVP-coated silver nanoparticles are stable for many days. The PVP on the surface of these monolayers can be exchanged by incubation in a solution of alkanethiols, allowing for a variety of functionalities to be displayed on the silver surface. This procedure was used for the displacement of adsorbed PVP by benzenethiol (BT), which readily forms a monolayer on metal surfaces, thus allowing for the quantitative analysis of the SERS enhancement factor.

The SERS enhancement factor (EF) is a quantitative measure of the Raman signal amplification of an analyte. We determined this value using the reported protocol[19] for similar sensing schemes: $EF = (I_{surface})/(I_{solution}) \times N_{surface}/N_{solution}$, where $N_{solution}$ and $N_{surface}$ are the number of molecules probed in a standard solution and on the substrate, respectively, and $I_{solution}$ and $I_{surface}$ correspond to the normal and SERS signal intensities, respectively. The number of molecules probed at the surface was estimated by dividing the total surface area of each of the nanocrystals by the van der Waals dimensions (2.3 Å × 2.3 Å) of the thiol head group, assuming benzenethiol forms a close-packed monolayer. This estimation represents one of the major sources of error in our EF calculation. To determine the EF for each of the close-packed arrays of particles, we examined Raman intensities for five different excitation wavelengths. Experiments were performed in a backscattering geometry, and multiple spectra taken over a 1-cm^2 substrate were averaged. The close-packed monolayers show consistent spectral responses across the entire sample, as shown in Figure 2. In general, our octahedra monolayers exhibit the largest EF (10^7–10^8 depending on wavelength). In contrast to several other SERS substrates, which show highly wavelength-dependant spectral responses,[20] intensities from a given sensor array vary by less than an order of magnitude as a function of wavelength. This behavior is attributed to interparticle interactions taking place in the close-packed arrays of nanoparticles. Previous work in our lab[13] and by others[21,22] has shown that as interparticle spacing decreases, plasmon coupling increases. The broad optical scattering profile of these substrates makes

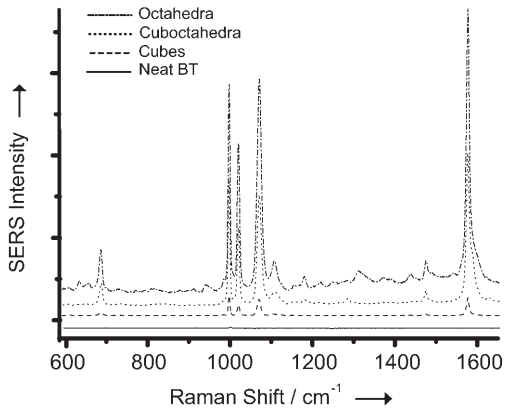

Figure 2. SERS spectra showing the response of benzenethiol-coated silver nanocrystal monolayers. Spectra are shifted vertically for clarity.

them more compatible with current hand-held Raman technology using readily available excitation sources.

Importantly, the variation in enhancement factors between close-packed arrays of these nanoparticle shapes also manifests itself in increased signal intensity for arsenate. As seen in Figure 3a, the variation in signal intensity for the

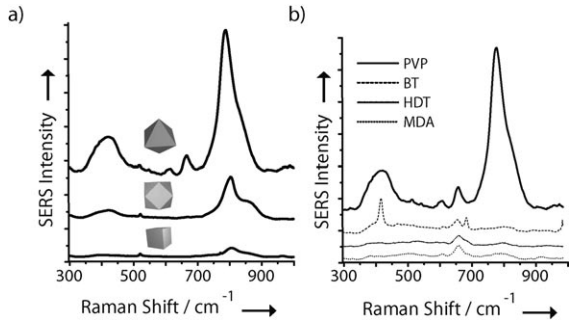

Figure 3. SERS spectra demonstrating the effect of shape and surface coating on arsenate signal intensity. a) SERS spectra collected on Langmuir–Blodgett films of each of the nanocrystal shapes coated with PVP and exposed to 1×10^{-6} M arsenate solution. Peaks at 800 and 425 cm^{-1} can be assigned to Na_2HAsO_4; all assignments are based on the literature.[23,24] b) SERS response of octahedra LB arrays coated with various organic species. BT: benzenethiol, HDT: hexadecanethiol, MDA: mercaptodecanoic acid.

arsenate solutions correlates to nanoparticle shape in the same fashion as the enhancement factor. For sensing experiments, the nanocrystal substrates are simply placed in contact with a droplet of the analyte solution within a 1-mm-thick plastic spacer and then covered by a glass cover slip. Figure 3a shows a typical SERS spectrum obtained for 18 ppb arsenate dissolved in water near each of the nanoparticle arrays coated with PVP. The intense peak at 800 cm^{-1} corresponds to the υ_1 (A_1) symmetric As–O stretch. The broad minor peak centered at 425 cm^{-1} is a superposition of υ_2 (A_1) and υ_5 (E) stretching modes of the arsenate molecule. The peak at 660 cm^{-1} in the SERS spectrum is associated with the C–C ring stretch of PVP (see the Supporting Information for PVP spectrum).

Because the distance between the silver surface and the analyte has been shown to play an important role in the sensitivity of SERS substrates,[25] a number of small-molecule capping agents were investigated in addition to PVP (Figure 3b). These capping ligands included benzenethiol, mercaptodeconoic acid, hexadecane thiol, and aminopropane thiol. In each case the PVP on the surface of the particle monolayers was exchanged by thiols in dilute ethanolic solution at room temperature. This exchange is not always complete, hence the minor peak at 660 cm^{-1} (residual PVP) persists. When compared with other surface coatings, PVP-coated particles give orders of magnitude stronger signal response from arsenate and greater stability to oxidation than the more commonly used citrate-coated silver nanoparticles[23] or sputtered silver films.[19] For each of the thiols tested, the Raman spectra showed very strong signal enhancement for the thiol coating, but little or no signal from the arsenic analyte in solution. In each of the thiol examples, it should be possible for the arsenate to come into close proximity of the nanoparticle surface, but even for thiols that can interact with arsenate through hydrogen bonds or electrostatics, no strong arsenate Raman signal can be collected. PVP seems to be an ideal coating for allowing arsenate ions close to the surface of the silver nanoparticles while still stabilizing the particles to oxidation.

For these substrates to be useful in the field detection of arsenic in groundwater, they must show good sensitivity for arsenate (the most abundant arsenic contaminant) at concentrations of 10 ppb or less. Although other SERS substrates, including sputtered silver films and silver colloidal solutions[23] can improve detection of the arsenate ion at high concentrations, our close-packed arrays of nanocrystals are the first to demonstrate SERS sensitivity significantly below 10 ppb (Figure 4a). The octahedral particles gave both the highest enhancement factor and best sensitivity for 1 ppb arsenate. For increasing concentrations between 1 and 180 ppb (Figure 4b), these substrates exhibit a linear dose response. This simple dependence allows for quantitative determination of arsenate concentration at levels that are an order of magnitude below current WHO guidelines. We note that recently a differential surface plasmon resonance sensing scheme based on an evaporated gold thin film was also reported with sensitivity for less than 1 ppb arsenic.[26]

Our sensing platform also provides a chemical fingerprint for the analytes, distinguishing between the two most common oxidation states of arsenic: arsenate (As^V) and arsenite (As^{III}). For an aqueous mixture of both arsenate and arsenite, both molecules can be detected simultaneously. A peak at 750 cm^{-1} corresponds to the ν_1 (A_1) symmetric As–O stretching mode for arsenite,[27] whereas the same stretching mode of arsenate appears at 800 cm^{-1} (Figure 5a). This

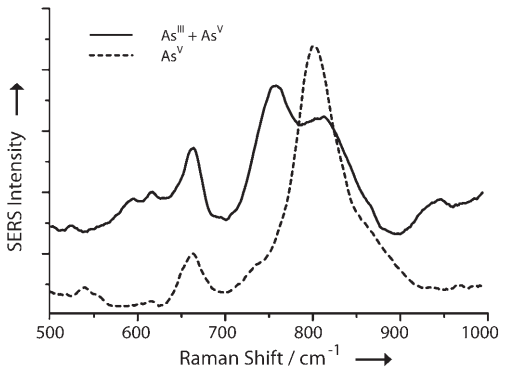

Figure 5. Chemical sensitivity of PVP-coated nanocrystal arrays. Speciation information obtained from SERS using an array of PVP-coated silver octahedral nanocrystals. The spectra were obtained for 18 ppb arsenate and arsenite solutions.

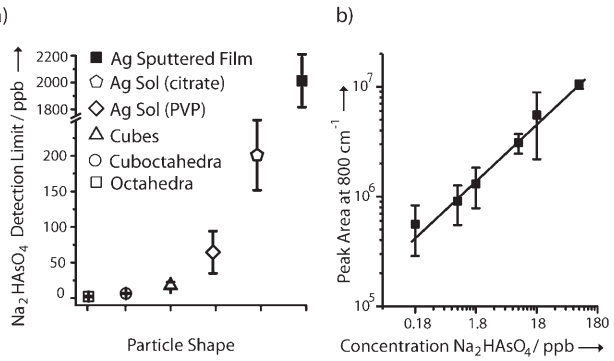

Figure 4. Characterization of the detection limit for arsenate on different substrates. a) Detection limit for arsenate sensing of each of the nanocrystal shapes along with a sputtered silver film and two types of silver colloidal solution-derived films for comparison. These values represent the lowest concentration at which arsenate peaks were distinguishable from the background. All shapes were assembled into LB arrays and were coated with PVP. The silver sols were prepared according to literature procedures and assembled by repeated drop casting. Error bars represent deviations between samples, which are much larger for the silver sols owing to sample variation and aging effects. b) A calibration curve for arsenate in water, which follows a linear trend between 1.0 and 180 ppb, indicating that this sensor is quantitative over a large concentration range.

chemical selectivity extends to other commonly found oxyanions in groundwater. Low arsenate concentrations (18 ppb) can be also detected even in the presence of high concentrations of sulfates (10 mM) and phosphates (1 mM).

The crucial verification of this sensitivity is further demonstrated by the ability to sense arsenic at low levels over a wide range of concentrations in real groundwater samples (Table 1). The SERS results were independently corroborated by AFS. To determine the arsenic concentration

Table 1: Detecting arsenic at low levels in real groundwater samples. A comparison of SERS sensing using the standard addition method to atomic fluorescence spectroscopy (AFS), demonstrating a very good agreement between these two methods of total arsenic detection.

SERS [ppb]	AFS [ppb]
116 (±15)	129
62 (±10)	51
38 (±6)	43
34 (±8)	31
21 (±4)	22
18 (±6)	12
6 (±3)	5

in the groundwater samples, a standard addition method was used to correct for matrix effects between samples. All of the SERS results fall within the one standard deviation of the AFS results, thus confirming the powerful ability of our SERS substrates to be used to sense arsenic quantitatively at very low levels.

In summary, the Langmuir–Blodgett assemblies of polyhedral Ag nanocrystals are highly active SERS substrates that can perform low-level arsenate and arsenite sensing in aqueous solutions. We achieve arsenate detection at 1 ppb—an order of magnitude below the current standard set by the WHO. Our SERS chip is robust, reproducible, highly portable, and could be easily implemented in field detection.

Experimental Section

All reagents and solvents were used as received from Aldrich, VWR, or Alpha Asear. Nanopure ($R > 18.0\ M\Omega$) water was purified with a Barnstead B-Pure system. Raman spectra were obtained using a Renishaw micro-Raman system microscope with a green diode-pumped solid-state laser at 532 nm as the excitation source. Also used was a multiple-wavelength Renishaw micro-Raman system with an Ar ion laser providing 488- and 514-nm lines, a 633-nm diode laser, and a 785 nm diode laser all operating with a power of approximately 2 mW at the sample. UV/Vis spectra were measured using an Agilent 8453 spectrophotometer. Scanning electron micrographs were obtained using a field emission scanning electron microscope (FESEM, JEOL6430) at the National Center for Electron Microscopy (NCEM). Images were obtained with an operating voltage of 3 KV.

Nanocrystal synthesis:[15] Silver nitrate (0.40 g) and copper(II) chloride (0.86 mg) were dissolved in 1,5-pentanediol (10 mL) in a glass vial. In a separate vial, PVP (MW = 55 000 amu, 0.20 g) was dissolved in 1,5-pentanediol (10 mL). Using a temperature-controlled silicone oil bath, 1,5-pentanediol (20 mL) was heated for 10 min at 193 °C. The two precursor solutions were then injected into the hot reaction flask at different rates: 500 μL silver nitrate solution every minute and 250 μL PVP solution every 30 s. For nanocubes, this addition was stopped once the solution turned opaque (ca. 6 min). For cuboctahedra and octahedra, the addition of precursor solutions was continued for a longer period of time (30–45 min for cuboctahedra and 60–75 min for octahedra). Citrate-coated silver sols were made according to the method used by Greaves and Griffith.[23] PVP-coated silver sols were made using a modified literature procedure,[28] wherein cold ($T = 4$ °C) 2 mM $NaBH_4$ in DI water (60 mL) was added to a cold stirring solution of 1 mM $AgNO_3$ (20 mL). This solution was allowed to warm to room temperature, at which time a 1 mg mL^{-1} solution of PVP (MW = 55 000 amu, 20 mL) was added. After 10 min of stirring, this solution was centrifuged (14 000 rpm for 10 min) and washed with EtOH three times to concentrate and remove excess PVP.

Nanoparticle purification: Average reactions yield product shape distributions in which the dominant shape represents 80–95 % of the sample, while many of the impurity shapes are larger polycrystals or wires. These larger impurities can be removed by vacuum filtration using progressively smaller Durapore filters (5.0, 0.65, 0.45, 0.22 μm) supported by a glass frit. To filter the particles, they are first transferred into a 0.02 wt % solution of PVP in water, where the final volume of this filtrate solution is ten times the volume of the original reaction solution. After filtration, the purified nanoparticle solutions are stored as suspensions in ethanol.

Nanoparticle assembly: Nanoparticle assembly was carried out using a Nima Technology LB trough. The nanocrystals were first transferred from ethanol to chloroform by centrifuging the ethanolic solution for 20 min at 3000 rpm and removing all but a few drops of the supernatant. The particles were then sonicated to bring them back into suspension, and chloroform was added dropwise to a volume of approximately 5 mL. The suspension of particles in chloroform was dispersed on the surface of the water dropwise, and the chloroform was allowed to evaporate for at least 0.5 h. The film was then compressed at 15 cm^2 min^{-1} until the surface pressure was 13.5 mN cm^{-2} (for dilute samples, lower surface pressure was used). This close-packed film was transferred to silicon substrates by a mechanical dipper moving at 2 mm min^{-1}.

Raman Spectroscopy: Benzenethiol-coated samples were prepared by first exchanging the PVP with BT in a 16 mM ethanolic solution that was stirred for 24 h at room temperature under a stream of N_2 to minimize oxidation. The samples were then thoroughly rinsed and dried under nitrogen before they were transferred to the microscope stage for immediate data collection. All sample collections were carried out with a 20× objective lens and were taken using ten-second scans between 400 and 1800 cm^{-1}.

Arsenic determination in groundwater: Samples of arsenic-contaminated groundwater were obtained from Professor Allen Smith (School of Public Health, UC Berkeley) and were used as received. Each unknown sample was analyzed using the standard addition method, wherein the unknown sample was doped with known amounts of arsenate while holding the volume constant. Then linear regression was performed on the resulting peak intensities to obtain the concentration in the unknown sample. For each groundwater sample, five samples were prepared, each of which contained 100 μL of the unknown sample. To this was added 0, 200, 400, 600, or 800 μL 1×10^{-5} M sodium arsenate in 18 MΩ deionized water. Finally, the volume of all five samples was normalized to 1 mL with 18 MΩ deionized water. Arsenate sensing was accomplished using a 1-mm plastic spacer on the LB substrates; a drop of liquid was put on the sample and covered with a cover slip. Spectra were then collected by averaging five ten-second scans obtained between 200 and 1000 cm^{-1} with a 532-nm diode laser operating with a power of approximately 20 mW at the substrate. Controls were performed to insure that the higher laser power was not degrading the PVP film in solution. At least five spectra were obtained for each sample, which were then analyzed using Microcal Origin software to run background subtraction and peak fitting routines. The peak intensity was plotted against the final added concentration of arsenate in the sample, and then the Origin linear regression routine (weighted for the standard deviation of each of the intensities) was used to obtain the equation of the line. The equation of the line was used to calculate the absolute value of the x-intercept, which is equal to the unknown concentration.[29] The error reported in the arsenic concentration represents the standard deviation in the x-intercept and was determined using the method described by Harris.[29]

Received: February 17, 2008
Published online: July 11, 2008

Keywords: arsenic · Raman spectroscopy · silver · surface effects · water analysis

[1] World Health Organization, Online Fact Sheet, **2007**, http://www.who.int/mediacentre/factsheets/fs210/en/.
[2] S. Richardson, T. Ternes, *Anal. Chem.* **2005**, *77*, 3807 – 3838.
[3] D. Melamed, *Anal. Chim. Acta* **2005**, *532*, 1 – 13.
[4] M. Wells, M. Gosh, R. Rigler, H. Harms, T. Lasser, J. R. van der Meer, *Anal. Chem.* **2005**, *77*, 2683 – 2689.
[5] B. Cullum, J. Mobley, Z. Chi, D. Stokes, G. Miller, T. Vo-Dinh, *Rev. Sci. Instrum.* **2000**, *71*, 1602 – 1607.
[6] D. Jeanmaire, R. VanDuyne, *J. Electroanal. Chem. Interfacial Electrochem.* **1977**, *84*, 1 – 20.
[7] M. Moskovits, *Rev. Mod. Phys.* **1985**, *57*, 783 – 826.

[8] S. Kawata, *Near-Field Optics and Surface Plasmon Polaritons*, Springer, Heidelberg, **2001**, pp. 15 – 27.
[9] J. Mock, M. Barbic, D. Smith, D. Schultz, S. Schultz, *J. Chem. Phys.* **2002**, *116*, 6755 – 6759.
[10] A. Michaels, J. Jiang, L. Brus, *J. Phys. Chem. B* **2000**, *104*, 11965 – 11971.
[11] K. Su, Q. Wei, X. Zhang, J. Mock, D. Smith, S. Schultz, *Nano Lett.* **2003**, *3*, 1087 – 1090.
[12] P. Jain, W. Qian, M. El-Sayed, *J. Phys. Chem. B* **2006**, *110*, 136 – 142.
[13] A. Tao, P. Sinsermsuksakul, P. D. Yang, *Nat. Nanotechnol.* **2007**, *2*, 435 – 440.
[14] D. Stuart, C. Yonzon, X. Zhang, O. Lyandres, N. Shah, M. Glucksberg, J. Walsh, R. VanDuyne, *Anal. Chem.* **2005**, *77*, 4013 – 4019.
[15] A. Tao, P. Sinsermsuksakul, P. D. Yang, *Angew. Chem.* **2006**, *118*, 4713 – 4717; *Angew. Chem. Int. Ed.* **2006**, *45*, 4597 – 4601.
[16] F. Kim, S. Connor, H. Song, T. Kuykendall, P. D. Yang, *Angew. Chem.* **2004**, *116*, 3759 – 3763; *Angew. Chem. Int. Ed.* **2004**, *43*, 3673 – 3677.
[17] Y. Sun, Y. Xia, *Science* **2002**, *298*, 2176 – 2179.
[18] A. Tao, F. Kim, C. Hess, J. Goldberger, R. He, Y. Sun, Y. Xia, P. D. Yang, *Nano Lett.* **2003**, *3*, 1229 – 1233.
[19] R. VanDuyne, J. Hulteen, A. Treichel, *J. Chem. Phys.* **1993**, *99*, 2101 – 2115.
[20] A. McFarland, M. Young, J. Dieringer, R. VanDuyne, *J. Phys. Chem. B* **2005**, *109*, 11279 – 11285.
[21] C. Chen, S. Tzeng, H. Chen, K. Lin, S. Gwo, *J. Am. Chem. Soc.* **2008**, *130*, 824 – 826.
[22] P. Jain, W. Huang, M. El-Sayed, *Nano Lett.* **2007**, *7*, 2854 – 2858.
[23] S. Greaves, W. Griffith, *J. Raman Spectrosc.* **1988**, *19*, 503 – 507.
[24] R. Frost, T. Kloprogge, M. Weier, W. Martens, Z. Ding, H. Edwards, *Spectrochim. Acta Part A* **2003**, *59*, 2241 – 2246.
[25] X. Zhang, J. Zhao, A. Whitney, J. Elam, R. VanDuyne, *J. Am. Chem. Soc.* **2006**, *128*, 10304 – 10309.
[26] E. Forzani, K. Foley, P. Westerhoff, N. J. Tao, *Sens. Actuators B* **2007**, *123*, 82 – 88.
[27] G. Pokrovski, J. Beny, A. Zotov, *J. Solution Chem.* **1999**, *28*, 1307 – 1327.
[28] J. Creighton, C. Blatchford, M. Albrecht, *J. Chem. Soc. Faraday Trans. 1* **1979**, *75*, 790 – 798.
[29] D. Harris, *Quantitative Chemical Analysis Sixth Edition*, Freeman, New York, **2002**, pp. 88 – 92.

